Influence of NaCl on Shape Deformation of Polymersomes

Rasangi M. Perera[1], Sudipta Gupta[1,7*], Tianyu Li[2], Markus Bleuel[3,4], Kunlun Hong[5,6], Gerald J. Schneider[1,8*]

[1]*Department of Chemistry, Louisiana State University, Baton Rouge, LA 70803, USA*

[2]*Department of Materials Science and Engineering, University of Tennessee, Knoxville, TN 37996, USA*

[3]*NIST Center for Neutron Research, National Institute of Standards and Technology, Gaithersburg, MD 20899-8562, USA*

[4]*Department of Materials Science and Engineering, University of Maryland, College Park, MD 20742-2115, USA*

[5]*Department of Chemical and Biomolecular Engineering, University of Tennessee, Knoxville, TN 37996, USA*

[6]*Center for Nanophase Materials Sciences, Oak Ridge National Laboratory, Oak Ridge, TN 37831, USA*

[7]*Department of Physics and Center for Soft Matter and Biological Physics, Virginia Tech, Blacksburg, VA 24061, USA*

[8]*Department of Physics & Astronomy, Louisiana State University, Baton Rouge, LA 70803, USA*

ABSTRACT

Polymersomes frequently appear in literature as promising candidates for a wide range of applications from targeted drug delivery to nanoreactors. From a cell mimetic point of view, it is important to understand the size and the shape changes of the vesicles in the physiological environment since that can influence the drug delivery mechanism. In this work we studied the structural features of polymersomes consisting of poly(ethylene glycol) - poly(dimethylsiloxane) - poly(ethylene glycol) at nanoscopic length scale in the presence NaCl, which is a very common

molecule in biotic aqueous environment. We used dynamic light scattering (DLS), cryo-TEM, small angle neutron and X-ray scattering (SANS/SAXS). We observed transformation of polymersome shape change from spherical to elongated vesicles at low salt concentration and in to multi-vesicular structures at high salt concentration. Model fitting analysis of SANS data indicated a reduction of vesicle radius up to 47 % and from the SAXS data we observed an increase in membrane thickness up to 8 % and an increase of the PDMS hydrophobic segment up to 11 % indicating stretching of the membrane due to osmotic imbalance. Also, from the increase in interlamellar repeat distance up to 98 % under high salt concentrations, we concluded that the shape and structural changes observed in the polymersomes are a combined result of osmotic pressure change and ion-membrane interactions.

Key words: vesicle, polymersomes, self-assembly, polymer-salt interaction, multi-vesicular

INTRODUCTION

Polymersomes are vesicular macro-assemblies of amphiphilic polymers. They are being studied extensively, for many important applications including but not limited to targeted drug/gene delivery[1 2], bioreactors[3-5], cell/viral capsid mimicking[6] and diagnosis.[7, 8] These vesicles have been shown to be more robust and less water permeable compared with phospholipid vesicles.[9] Polymersomes can be designed to meet specific requirements such as size, membrane structure, shape, surface activity and response toward internal and external stimuli.[10] Several pioneering studies can be summarized as follows. A pH responsive polymersome, consists of CS-poly(β-amino) ester have been studied by Xu et al for co-delivering hydroxychloroquine (HCQ) and tunicamycin (Tuni) drugs to achieve an antitumor effect and inhibiting tumor metastasis.[11] Liu et al. have reported a study based on a PVCL-PDMS-PVCL polymersome, which has a temperature

controlled permeability with a sustained delivery of anticancer drug Doxorubicin (DOX).[12] When considering polymersomes as drug delivery vesicles from a cell mimetic point of view, we can conclude that the shape and size of the polymersomes have strong impact of its performance such as biodistribution, pharmacokinetic properties and cell internalization.[13-20] For example, while disk-like red blood cells with dimensions of 6-8 μm routinely pass through the spleen, spherical particles must be less than 200 nm in diameter to do the same.[21] According to Champion et. al., speed of phagocytosis of IgG-opsonized anisotropic polystyrene particles by alveolar macrophages depends on the local particle shape at the point of initial contact.[20] Shape transformation of polymersomes can be achieved by osmotic pressure change, chemical structure change, temperature change or by applying a pH cahnge.[22-25] As polymersome membranes can act as highly sensitive barrier an osmotic pressure gradient may occur between inside and outside. Also, different ions can interact with the membrane.[26] This may lead to potential shape deformations of the vesicles.[22, 27] Therefore, it is important to study how the osmotic pressure and the interaction of different ions with the membrane affect the shape changes so that we can advance the understanding the behavior of polymersomes when they are introduced into biological environments. In addition, by understanding the fundamental processes imposed by osmotic pressure and ion – membrane interactions, we may be able to decide polymer size, hydrophilic/lipophilic ratio, and the architecture for designing a new type of polymersome with accurate control of the shape deformation that leads to optimized design. This will help to obtain control over the polymersome shape and understand the mechanism of the shape change.

Most theoretical studies explaining vesicle shape transformation are based on liposomes consist of lipid molecules. Numerous vesicle shape transformation pathways have been proposed using the data obtained from studies involving lipid vesicles where spherical vesicles change their shapes to

tubular, oblate and stomatocytes etc. as a response to changes in volume-to-area ratio, $v = \frac{V}{\left(\frac{4\pi}{3}\right)R_0^3}$ (where $R_0 = (A / 4\pi)^{1/2}$ is the radius of a sphere with the same area) and area difference, $\Delta A = A_{in} - A_{out}$.[28-30] Provided that the triblock copolymer chains having an ABA arrangement (hydrophilic−hydrophobic−hydrophilic), adapt I-shape conformations inside the self-assembled membrane, where the hydrophobic block forms a stretched/elongated chain resulting in a monolayer-like membrane structure (Figure 1), we can assume the same shape transformation pathways to explain the polymersome shape changes. Vesicles adjust their shapes in a way that minimizes the bending energy, E_b. According to the spontaneous curvature model of Helfrich, $E_b = \frac{\kappa}{2}\phi\,(2C - C_0)^2 dA$, depends on three parameters: bending rigidity $(\boldsymbol{\kappa})$, mean surface curvature $(\boldsymbol{C})$ and spontaneous curvature (C_0).[2, 26, 31] Bending rigidity is governed by the chemical properties of the membrane, (thus by composition and length of the polymer chains) as well as the surrounding environmental factors (temperature and solvent composition). The mean surface curvature will depend upon the degree of curvature at different positions of the membrane and is subjected to change with the shape. Spontaneous curvature (C_0) on the other hand does not depend on the shape; rather it is sensitive to the membrane microenvironment.[32] A positive C_0 would favor the shape change to prolates and tubes and a negative C_0 would favor the oblates, disks and stomatocytes.[2]

It has been shown by Coarse-grained (CG) based molecular dynamics simulations, that under low stress conditions, polymersome shape change is governed by membrane stretching where polymersome contracts symmetrically and maintains a symmetrical shape. After a certain threshold limit polymersome shape is governed by membrane bending and generates non-spherical shapes.[33] The shrinkage reduces the osmotic pressure but increases the bending energy, E_b. At a certain point bending energy will be the determining parameter for the shape. To minimize the

bending energy, polymersome should adjust the surface area difference (ΔA) and obtain a final kinetic shape. But osmotic pressure alone cannot explain all the shape changes observed at different hypertonic conditions and we need to consider membrane-ion interactions too. There are few reports available in literature that discuss the combined effect of osmotic pressure and solute-membrane interactions on the shape change of polymersomes and studies done at high salt concentrations are even less.[26, 27, 34] In this context we focused on a holistic approach to discuss the impact of NaCl on the shape deformation of the biocompatible[35, 36] PEG-PDMS-PEG polymersomes and the structure-property relationship that may change. Poly (ethylene glycol) (PEG) is one of the most used polymers in medical and biological applications due to its non-toxicity, non-immunogenicity, and biocompatibility. It is also one of the few FDA approved polymers.[36] PDMS is widely used as an optically clear, flexible, inert, nontoxic, non-flammable biocompatible material, and it is routinely used as a biomedical implant material and for fundamental cellular studies.[35] Na^+ is the major cation and Cl^- is the major anion in the extracellular fluid and present in the concentration range of roughly 100−150 mM.[37] NaCl solutions ranging from 0 to 500 mM concentrations were used to induce the osmotic imbalance in the polymersome solution and the structural characterizations were done using dynamic light scattering (DLS), cryogenic transmission electron microscopy (cryo-TEM), small-angle X-ray scattering (SAXS) and small-angle neutron scattering (SANS).

DATA MODELING

Polymersome structure: The polymersome form factor is modeled using an extension of the core-multi shell model used in our previous studies.[38-41] The core is filled with water and in case of multi-vesicular polymersomes encapsulated by N shells of PEG-PDMS-PEG and $N-1$ layers of solvent as illustrated in Figure 1 a. We can model the data using a core of radius R_c and $n = 3N + 1$

shells for each layer of PEG, PDMS, PEG, and water. Each shell thickness and scattering length density is assumed to be constant for the respective shell. The 1D scattering pattern is described by:

$$P(Q,R,t,\Delta\rho) = \frac{\phi[A(Q)]^2}{V(R_{SANS})} \quad (1)$$

with the scattering amplitude *A(Q)* is given by a simplified core-multi-shell model

$$A(Q) = (\rho_{\text{solv}} - \rho_c)3V(R_c)\frac{j_1(QR_c)}{QR_c} + \sum_{i=1}^{3N+1}\left[(\rho_i - \rho_c)3V(r_i)\frac{j_1(Qr_i)}{Qr_i}\right] \quad (2)$$

For a spherical Bessel's function $j_1(x) = \frac{\sin(x) - x\cos(x)}{x^2}$, $V(r)$ is volume of the sphere with radius *r* given by $V(r) = \frac{4}{3}\pi r^3$, with, ϕ, the corresponding polymer volume fraction. Here the outer radius is given by $r_i = R_c + it_j$, with t_j will be the thickness of the PEG (δ_{PEG}), PDMS (δ_{PDMS}), PEG (δ_{PEG}) and interlayer water thickness (t_w), for i = 1, 2, 3, and 4 respectively and repeating itself. Therefore, for N = 2 layers we have n = 3N + 1 = 7 layers of shells consisting of 2 layers of PEG-PDMS-PEG and 1 interlayer water. The outer perimeter radius is $R_{SANS} = R_c + \delta_M$, with membrane thickness, $\delta_M = (N-1)t_w + 2N\delta_{PEG} + N\delta_{PDMS}$. The corresponding neutron scattering length density (NSLD) is given by ρ_i. For PEG-PDMS-PEG polymersome we used the scattering length density of the shell, $\rho_{\text{PEG}} = 0.634 \times 10^{-6}$ Å^{-2}, $\rho_{\text{PDMS}} = 0.063 \times 10^{-6}$ Å^{-2}, and for D_2O the NSLD of the solvent core is given by, $\rho_{\text{solv}} = \rho_c = 6.36 \times 10^{-6}$ Å^{-2}. The macroscopic scattering cross-section is obtained by,

$$\frac{d\Sigma}{d\Omega}(Q) = \int drP\left(Q,R,t,\rho_{\text{polymer}},\rho_{\text{solv}}\right)s(r) \quad (3)$$

For the size polydispersity, a log-normal distribution following the size distribution we obtain from DLS. In addition, the thickness of the shell and the solvent are convoluted with a Gaussian distribution function to account for the thickness polydispersity. A more detailed modeling for unilamellar polymersome and the size distribution is reported in the supplemental information (SI).

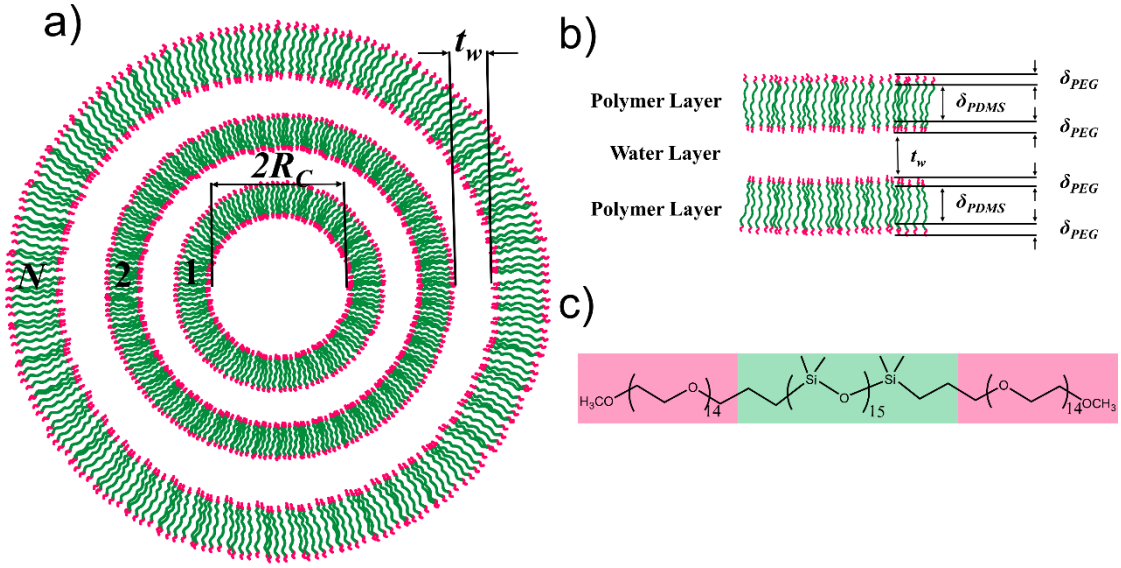

Figure 1. Schematic representation of (a) the multivesicular polymersome, structure illustrating the number of bilayers, N, the radius of the core, R_c, the (b) thickness of the PEG shells, δ_{PEG}, the thickness of the interleaved solvent layers, t_w and the thickness of the PDMS shell, δ_{PDMS}, (c) Chemical structure of triblock copolymer.

Membrane structure: The random lamellar sheet consisting of the PEG and PDMS moieties of the tri-block copolymer forming the PEG-PDMS-PEG membrane can be modelled using the Caille structure factor.[42, 43] It provides direct access to the macroscopic scattering cross-section given by the scattering intensity for a random distribution of the lamellar phase, as

$$\frac{d\Sigma}{d\Omega}(Q) = 2\pi \frac{\phi P(Q) S(Q)}{Q^2 d} \quad (4)$$

with the particle volume fraction, ϕ, and the distance of the lamellae, d. The form factor is given by:

$$P(Q) = \frac{4}{Q^2}\left[\Delta\rho_{PEG}\left\{\sin(Q(\delta_{PEG} + \delta_{PDMS})) - \sin(Q\delta_{PDMS})\right\} + \Delta\rho_{PDMS}\sin(Q\delta_{PDMS})\right]^2 \quad (5)$$

The scattering contrasts for the PEG and PDMS parts are $\Delta\rho_{\mathrm{PEG}}$ and $\Delta\rho_{\mathrm{PDMS}}$, respectively. The corresponding thicknesses are δ_{PEG} and δ_{PDMS}, respectively, as presented in Figure 1. The PEG-PDMS-PEG membrane thickness is given by, $\delta_{HH} = 2(\delta_{PEG} + \delta_{PDMS})$. For unilamellar structure, $N = 1$, the repeat distance in equation 4 is given by the membrane thickness, δ_{HH}. The PEG and PDMS contrast are given by $\Delta\rho_{PEG} = \rho_{\mathrm{PEG}} - \rho_{\mathrm{solv}}$, and $\Delta\rho_{PDMS} = \rho_{\mathrm{PDMS}} - \rho_{\mathrm{solv}}$, respectively. The corresponding X-ray scattering length densities (XSLD) are given by $\rho_{\mathrm{PEG}} = 10.45 \times 10^{-6}$ Å^{-2}, $\rho_{\mathrm{PDMS}} = 8.92 \times 10^{-6}$ Å^{-2}, and for D_2O as solvent $\rho_{\mathrm{solv}} = 9.34 \times 10^{-6}$ Å^{-2}.

The Caille structure factor for $N > 1$ is given by,

$$S(Q) = 1 + 2\sum_{n=1}^{N-1}\left(1 - \frac{n}{N}\right)\cos(Qdn)\exp\left(-\frac{2Q^2d^2\alpha(n)}{2}\right) \quad (6)$$

with the number of lamellar plates, N, and the correlation function for the lamellae, $\alpha(n)$, defined by

$$\alpha(n) = \frac{\eta_{\mathrm{cp}}}{4\pi^2}\left(\ln(\pi n) + \gamma_E\right) \quad (7)$$

with γ_E = 0.57721 the Euler's constant. The elastic constant for the membranes is expressed in terms of the Caille parameter, $\eta_{\mathrm{cp}} = \frac{{Q_0}^2 k_B T}{8\pi\sqrt{\kappa_b\,\kappa_A}}$, where κ_b and κ_A are the bending elasticity and the compression modulus of the membranes, respectively. Here κ_A is associated with the interactions between the membranes. The position of the first-order Bragg peak is given by Q_0, and k_B is the Boltzmann's constant and T the absolute temperature.

EXPERIMENTAL SECTION

Materials

All chemicals and reagents were used as received. Allyloxy (polyethylene oxide), methyl ether and hydride terminated poly(dimethylsiloxane) was purchased from Gelest Inc (Morrisville, PA), Anhydrous toluene and Karstedt's catalyst were purchased from Sigma-Aldrich (St. Louis, MO).

Synthesis of PEG-b-PDMS-b-PEG Triblock Copolymer

PEG_{14}-$PDMS_{15}$-PEG_{14} triblock copolymer was synthesized by hydrosilylation between different blocks: Hydride terminated poly(dimethylsiloxane) with a number average molecular weight of 1100 g/mol as hydrophobic block and allyloxy (polyethylene oxide), methyl ether with a number average molecular weight of 600 g/mol as the hydrophilic block (Figure S1). Average molecular weights of each individual blocks were determined by MALDI TOF/TOF MS (Figure S2). Hydride terminated PDMS (8.0 g, 7.3 mmol, 1 eq), allyloxy (polyethylene oxide), methyl ether (9.7 g, 16.1 mmol, 2.2 eq), Karstedt's catalyst solution (0.89 mL, 30 ppm) and anhydrous toluene (100 mL) were charged into a 250 mL three-neck round bottom flask under inert atmosphere. Then, the reaction was heated at 70°C overnight. After removing of solvent, the obtained polymer was

purified by dialysis in methanol using a dialysis membrane with Molecular Weight Cutoff (MWCO) of 1000 Da to remove excess PEG. The final product was filtered with a 0.1 μm filter to remove the Pt from Karstedt's catalyst. The success of the coupling between PDMS and PEG blocks was confirmed by ^{1}H NMR by the disappearance of terminal H signal of PDMS and the signal shift of terminal H of PEG upon the reaction. Further, the disappearance of H signal from double bond in PEG confirmed that no excess PEG remained in the final product. (Figure S3).

Polymersome Preparation

Polymersomes were obtained by direct dissolution of polymer in D_2O at 4 mg/ml concentration. Then the solution was subjected to 30 seconds of sonication using a Sonic Vibra Cell VC 750 transducer and probe under 20% amplitude. The triblock copolymer having a hydrophilic mass fraction of 0.52 self-assembled into vesicles.[28] To obtain monodisperse unilamellar vesicles, the resulted solution was double extruded through a 0.1 μm pore size polycarbonate membrane using a double-syringe mini-extruder. (Both membrane and extruder were purchased from Avanti Polar Lipids, Alabaster, AL, USA.). Polymersome solutions were mixed with NaCl solutions in 1:1 ratio to obtain the desired external salt concentration and final polymer concentration of 2 mg/ml in a 1 ml volume. The measurements were done 24 hours after the sample preparation which has shown to be sufficient to reach equilibrium and keeping at ambient temperature, 25°C.

Dynamic Light Scattering

Dynamic light scattering (DLS) measurements were performed using a Malvern Zetasizer Nano ZS equipped with a He-Ne laser of wavelength, λ = 633 nm at 30 mW laser power, at a scattering angle θ = 173 °. The hydrodynamic radius, R_h, of the polymersomes in each NaCl concentration was calculated using the Stokes-Einstein equation, $R_h = k_B T/(6\pi\eta_0 D)$, with the Boltzmann

constant, k_B, the temperature, T, the viscosity of the solvent (D_2O or NaCl solution), η_0. Three separate DLS measurements for each mixture were averaged.

Cryo-Transmission Electron Microscopy

Cryogenic-transmission electron microscopy (cryo-TEM) images were recorded on a Tecnai G2 F30 operated at 150 kV. A volume of ten microliters of the sample (2mg/ml polymersome: in pure D_2O, or NaCl) was applied to a 200 mesh lacey carbon grid mounted on the plunging station of an FEI Vitrobot™ and excess liquid was blotted for 2 s by the filter paper attached to the arms of the Vitrobot. The carbon grids with the attached thin film of polymersome suspensions were plunged into liquid ethane and transferred to a single tilt cryo - specimen holder for imaging. By quick plunging into liquid ethane, the vesicles are preserved at their hydrated state present at room temperature. Cryo-TEM images were obtained in the bright field setting.

Small Angle Neutron Scattering

Small-angle neutron scattering (SANS) experiments were conducted at the NG 7 SANS instrument of the NIST Center for Neutron Research (NCNR) at National Institute of Standards and Technology (NIST).[44] The sample-to-detector distances, d, were fixed to 1, 4, and 13 m, at neutron wavelength, λ = 6 Å. Another configuration with lenses at d = 15.3 m, and λ = 8 Å was used to access low Q's.[45] This combination covers a Q - range from ≈ 0.001 to ≈ 0.6 Å^{-1}, where $Q = 4\pi \sin(\theta/2)/\lambda$, with the scattering angle, θ. A wavelength resolution of, $\Delta\lambda/\lambda$ = 14%, was used. All data reduction into intensity, $I(Q)$, vs. momentum transfer, $Q = |\vec{Q}|$ was carried out following the standard procedures that are implemented in the NCNR macros for the Igor software package.[46] The intensity values were scaled into absolute units (cm^{-1}) using direct beam. The solvents and empty cell were measured separately as backgrounds.

Small Angle X-ray scattering

Small-angle X-ray scattering (SAXS) experiments were conducted at the Bio-SAXS beamline at the Stanford Linear Accelerator Center (SLAC) facility. At the synchrotron instrument, the samples were measured in a flow cell with an acquisition time of 1 s, whereas the samples were loaded in 1 mm borosilicate glass capillary cylinders for the lab X-ray with an acquisition time of 10 s. The recorded intensities were corrected for dark current, empty cell and solvent (buffer) using standard procedures.[47] [48] The scattering intensity was normalized to absolute units (cm^{-1}) using water as calibration standard.[49] The energy at the SLAC source was 11 keV.

RESULTS AND DISCUSSIONS

Polymersome size, morphology, and structure

DLS data showed a rapid decrease of hydrodynamic diameter (D_h) with changing NaCl concentration, ϕ_M, from 1 to 5 mM (Figure 3). Then D_h is almost constant until the external NaCl concentration reaches up to 150 mM. Another rapid decrease of D_h was observed at 250 mM and 500 mM concentrations. The change in D_h is attributed to osmotic shrinkage of vesicles or shape changes.[50, 51] The addition of salt can create an osmotic pressure difference, Π, across the polymersome membrane, $\Pi = RT\ (\Delta\phi_M)$, causing shrinkage or reduction in volume of the vesicle and transferring water through the membrane. Here R is the gas constant, $\Delta\phi_M$ is the concentration difference of the solute across the membrane, and T is the absolute temperature.

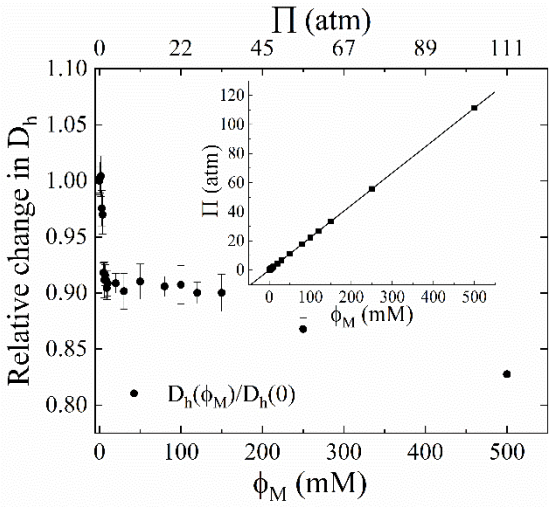

Figure 2. Relative change of hydrodynamic diameter $D_h = D_h(\phi_M)/D_h(0)$ *of the polymersomes with external NaCl concentrations,* ϕ_M *and osmotic pressure,* Π*.* $D_h(0)$ *is the initial diameter of the polymersome under isotonic conditions. Inset, linear dependence of* Π *with* ϕ_M *following* $\Pi = RT\ (\Delta\phi_M)$*, presented by the solid line.*

To get direct images and examine the structural information polymersomes - salt systems cryo-TEM experiments were done for selected NaCl concentrations (5 mM, 100 mM, and 250 mM). The cryo-TEM images (Figure 4) demonstrated that all salt concentrations can induce shape changes to the polymersome. At 5 mM NaCl concentration, counting n = 73 particles revealed that 50.7 % of the structures were elongated tubular shaped vesicles, 38.4 % were spheroids, and 11 % nested vesicles. At 100 mM NaCl concentration (n = 52), 48 % of the vesicles had spheroidal shape and 38.5 % appeared as multivesicular vesicles.[52, 53] Rest, 13.5 % were nested vesicles. For the 250 mM NaCl concentration multivesicular vesicles were the most abundant with 31 % of the total vesicles (n = 50) and 15 % had spheroidal shape. Very small number of nested vesicles (4 %) and elongated tubular vesicles (2 %) were also present. Aspect ratio analysis shows deviation of spherical shapes started even for 5 mM NaCl concentration. Details are presented in the supplemental information.

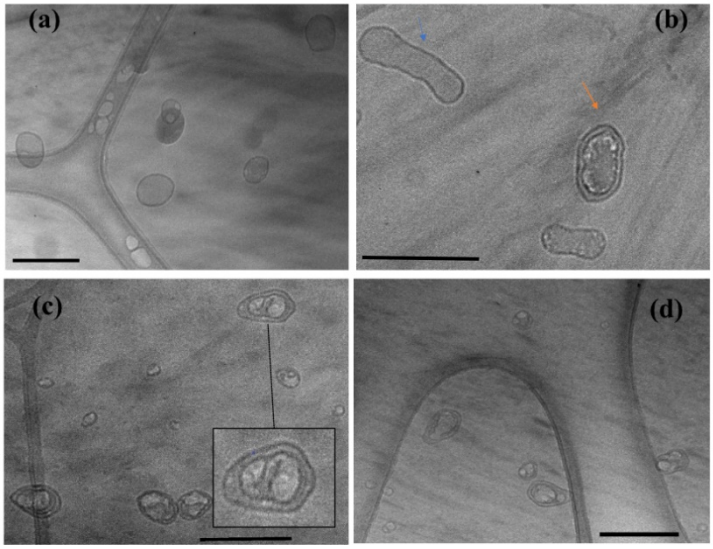

Figure 3. Cryo - TEM images of polymersomes (a) in their original state, under (b) 5 mM. Blue arrow indicates an elongated tubular vesicle, orange arrow indicates a nested vesicle. (c) 100 mM. Inset: zoomed image of a multivesicular vesicle. (d) 250 mM NaCl concentrations. Scale bar represents 200 nm.

The polymersome structure is investigated using SANS to obtain the statistically dominant one, after averaging over many particles, the size of the core, shell, and membrane thickness. **Error! Reference source not found.** a illustrates the SANS data for the pure polymersome at 0 mM NaCl concentration, whereas the scattering contribution from the PEG, PDMS, and total scattering from the modified core-shell model are presented. The detailed data modeling for $N = 1$ layer as a special case for equations 1 - 3 can be found in the supplemental information, where we have discussed in details the scattering contributions from different cross terms as suggested by earlier work.[54] In **Error! Reference source not found.** b we present the neutron scattering profile as a product of the NSLD and the number density (N_{agg}/V_{SANS}) as function of particle radius, R_{SANS}, occupying a volume of V_{SANS}. The data is plotted with respect to solvent (D_2O) NSLD, so that outside the membrane thickness we have only D_2O NSLD as the background. The corresponding aggregation

number, N_{agg}, gives the number of polymers per polymersome. We have used a compact core-shell model (equations 1- 3) with a given shell volume of V_{shell}, we have $N_{agg} = V_{shell}/(2Nv_{PEG} + Nv_{PDMS})$, where v_{PEG}, and v_{PDMS} are the molar volume of the PEG and PDMS blocks, respectively.

The SANS diffraction data for different salt concentrations are illustrated in Figure 5 and the solid lines represents the fits following equations 1 - 3. All the data over a range from 5 to 500 mM are modelled for N = 2 layers, using a lognormal polydispersity for the water core and Gaussian polydispersity for the inter-layer water thickness. The fitting parameters are reported in Table 1. Starting with the 0 mM sample we observed a systematic decrease in the overall radius from SANS with increase in NaCl concentration. The membrane thickness, δ_M, decreases by 13% at 5 mM, and seems to stay constant within the experimental accuracy, with and eventual increase to 5.9 nm at 500 mM concentration, which indicates recovery to the original δ_M at 0 mM. Similar behavior was observed in lipid bilayer vesicles.[55, 56] It was suggested that at low NaCl concentration the electrostatic repulsive force is too weak, and the external osmotic pressure causes a decrease in membrane thickness. However, with increase in NaCl concentration the electrostatic repulsive force causes a slight increase in membrane thickness. In case of lectin bilayers it was reported that salt induced osmotic pressure can reduce the inter-bilayer water thickness until a saturation is reached that balances this osmotic stress with inter-bilayer repulsive force.[57] We observed a similar decrease in the inter-bilayer water thickness, t_w, with increase in external osmotic pressure.

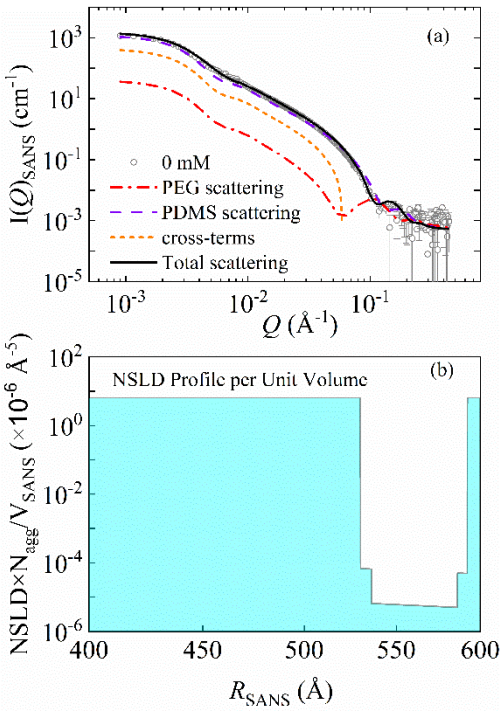

Figure 4. (a) SANS scattering intensity for 0 mM NaCl concentrations of PEG-PDMS-PEG polymersome dispersed in D_2O. The solid lines represent fits using the model introduced by equation 1-3. The contribution from PEG, PDMS and total scattering are depicted. (b) Corresponding neutron scattering length density times polymer number density (N_{agg}/V_{SANS}) as a function of particle radius. Here, N_{agg}, the aggregation number and, V_{SANS}, the particle volume.

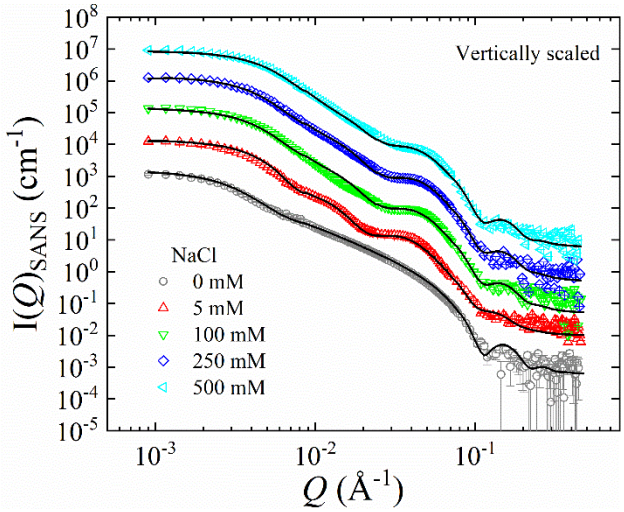

Figure 5. SANS scattering intensity for various NaCl concentrations added from outside on PEG-PDMS-PEG polymersome dispersed in D_2O. The data vertically scaled for better visualization. The solid lines represent fits using the model introduced by equation 1-3.

When compared the results from SANS and DLS at different NaCl concentration we observed a decrease in outer radius (*cf*. Figure S 11 in the SI). The ratio between the hydrodynamic radius and SANS radius, R_h/R_{SANS} varies from 1.1 to 1.8 for ϕ_M ranging from 0 to 500 mM. The large difference between R_h and R_{SANS} for polymersome has been reported in the literature.[58-60] This can be attributed to the high polydispersity in size and shape, observed from shape and aspect ratio analysis of cryo-TEM images (Figure 03 & Figure S5). R_h is shifted to higher values by polydispersity.[58] Further, it was reported that due to large hydration effect the NSLD of the PEG block in the polymersome becomes close to that of D_2O, so that, $\Delta\rho^2 = \rho_{\text{hydrated}-\text{PEO}} - \rho_{\text{D2O}} \approx 0$.[58] As an example of this effect we found that the PEG thickness of the polymersome from SANS, $\delta_{PEG} = 0.6 \pm 0.1$ nm is much smaller than radius of gyration, $2R_g = 1.7$ nm, of linear PEG chain of M_w = 600 g/mol in good solvent.[61] Therefore, compared to DLS we see only a part of the PEG chain from SANS, which could potentially explain $R_{\text{SANS}} < R_{\text{DLS}}$.

It should be noted that in case of polybutadiene-b-poly(L-glutamicacid), PB_{48}-b-PGA_{114} vesicles consisting of dense compact PB core and polyelectrolyte PGA shell a $R_h/R_{SANS} \approx 4.5$ was reported in the literature.[59] The variety of shapes and diameters, including the nested objects observed by cryo-TEM (Figure 3) could be the potential reason for the large polydispersity of 38% needed to explain SANS data, Table 1.

Membrane structure

Hereafter, we study the structure factor of the shells more in detail taking advantage of the good resolution of small-angle X-ray scattering (SAXS). Figure 6 a represents the SAXS data for 0 mM NaCl concentration, where we compare the data modelling from the core-shell model for ULV used for SANS (equation S1 in the SI) and the membrane model (equations 4 - 5). We did not observe any contribution from the Caille Structure factor, i.e., $S(Q) = 1$ in equation 4 and the data

is modeled using unilamellar, N=1, membrane structure. For this particular case, SANS and SAXS data can be conveniently described by the core-shell models introduced to analyze the SANS data. As the Q-range of the SAXS experiments is limited to higher Q, fitting required to keep the particle size constant with the value obtained from the SANS fit. As a result, we find that the fitting parameters for the thickness of the PEG and PDMS layers from the core-shell and membrane model are the same as reported in Table 2, within standard deviation of the analysis.

Table 1. Parameters obtained from SANS analysis. For different NaCl concentration, ϕ_M, the number of layers in MLVs, N, the outer perimeter radius, R_{SANS}, the PEG-PDMS-PEG membrane thickness, δ_M, the thickness of the water layer between the membranes t_w, log-normal and Gaussian polydispersity for R_{SANS} and t_w, are given by $PD_{LN}(R_{SANS})$ and $PD_G(t_w)$ respectively. The aggregation number is given by N_{agg}. Some parameters are not applicable (NA) for N = 1.

ϕ_M (mM)	N	R_{SANS} (nm)	δ_M (nm)	t_w (nm)	$PD_{LN}(R_{SANS})$	$PD_G(t_w)$	N_{agg}
0	1	59.2 ± 2	6.2 ± 0.9	NA	0.30 ± 0.02	NA	65954 ± 128
5	2	42.7 ± 1	5.5 ± 0.8	6.7 ± 0.3	0.35 ± 0.03	0.60 ± 0.002	48490 ± 261
100	2	34.6 ± 1	5.8 ± 0.2	5.6 ± 0.2	0.53 ± 0.02	0.61 ± 0.002	26855 ± 208
250	2	34.5 ± 1	5.9 ± 0.4	5.2 ± 0.1	0.60 ± 0.02	0.79 ± 0.003	24172 ± 198
500	2	31.0 ± 1	5.9 ± 0.4	5.2 ± 0.1	0.61 ± 0.03	0.79 ± 0.003	18355 ± 180

The scattering contribution from the PEG, PDMS and total scattering is depicted using equations 4 - 5. The contribution of the cross term is presented in the SI. The corresponding XSLD profile convoluted with Gaussian distribution for PEG, PDMS thickness is illustrated in Figure 6 b as a function of the particle radius given by $R_c + \delta_M + (N-1)t_w$, calculated from the water core

radius, R_c, from SANS whereas, the membrane thickness, δ_M, and water thickness, t_w, calculated from SAXS.

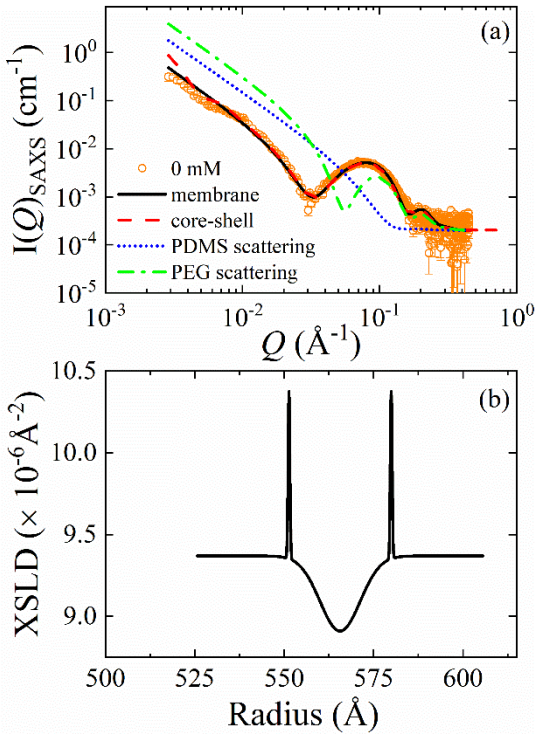

Figure 6. (a) SAXS data for 0 mM NaCl concentrations. The contribution from PEG, PDMS and membrane scattering using equations 4 - 5 is depicted. It is also compared with the core-shell model for ULVs described in equation S1 in the SI. (b) The corresponding X-ray scattering length density (XSLD) profile along particle radius calculated from the water core radius, R_c, from SANS whereas, the membrane thickness, δ_M, and water thickness, t_w, calculated from SAXS as described in the text.

Figure 7 represent the SAXS data for different NaCl concentrations. We start observing multi-vesicular structure, $N = 2$, for $\phi_M \geq 5$ mM. The solid lines represent the data modeling using equations 4 - 7. The fitted parameters are reported in Table 2. Similar to the results from SANS in comparison to 0 mM sample from SAXS we observed 8% initial decrease in the membrane thickness, δ_M, followed by an increase and almost recovers back the initial δ_M at 0 mM. However, the δ_M, obtained from SAXS is larger than that of SANS. This is due to the fact that we can now

see the PEG thickness no longer masked by the partial matching of NSLD due to hydration effect from water. In fact, for 0 mM sample δ_{PEG} = 1.4 nm which is close to $2R_g = 1.7$ nm, for linear PEG chain in aqueous solution. For ϕ_M ranging from 0 to 500 mM, the PDMS block is stretched ranging from 4.2 to 4.7 nm. This is close to the mean chain end-to-end distance, $\langle R_{ee} \rangle$ = 5 nm for PDMS of M_n = 1100 g/mol and agrees well with previously reported values of membrane thicknesses of polymersomes composed of similar triblock copolymer with PDMS as the central hydrophobic block[62, 63] According to Etel *et al* the repulsion between the hydrophilic and the hydrophobic block causes a more stretched chain conformation.[64] This could explain the PDMS block length. Additionally, the polymersome membrane thickness is close to the membrane thickness values reported for liposomes for which salt induces structural changes have been reported abundantly.[37, 65-67] This will be useful when comparing lipid vesicle systems with reported polymer vesicle system.

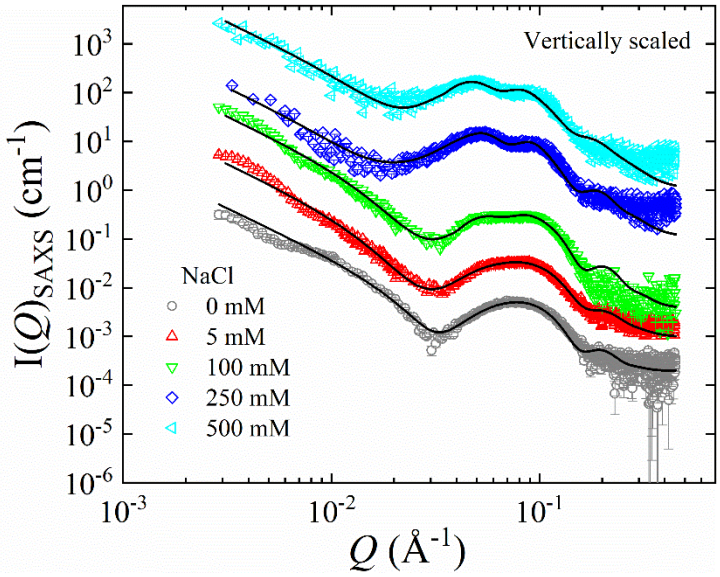

Figure 7. The SAXS data for various NaCl concentrations ranging from 0 to 500 mM. The data vertically scaled for better visualization. The solid lines are the model as described in equations 4 - 7.

The Caille parameter η_{cp} has been kept constant at 0.001 and appears to have negligible effect on the polymersome S(Q) peak in bulk aqueous solutions. However, the S(Q) peak becomes sharper with increase in NaCl concentration that has been modeled by the decrease in Gaussian polydispersity for the lamellar repeat distance given by $PD_G(d)$. On increasing ϕ_M from 0 mM to 500 mM the polydispersity corresponding to PDMS thickness, $PD_G(\delta_{PDMS})$, increases by 58%. This is attributed to the formation of nested polymersome structures as observed from cryo-TEM (Figure 3).

Table 2. Parameters obtained from SAXS analysis. For different NaCl concentration, ϕ_M, the number of layers, N, average lamellar spacing, d, thickness of the PEG layer, δ_{PEG}, thickness of the PDMS layer, δ_{PDMS}, the thickness of the PEG-PDMS-PEG membrane δ_M and the Gaussian polydispersity index for d and δ_{PDMS} are given by $PD_G(d)$ and $PD_G(\delta_{PDMS})$, respectively. For N = 1 (ULV) d is kept fixed to δ_M.

ϕ_M (mM)	N	d (nm)	δ_{PEG} (nm)	δ_{PDMS} (nm)	δ_M (nm)	$PD_G(d)$	$PD_G(\delta_{PDMS})$
0	1	7.13	1.429 ± 0.001	4.274 ± 0.003	7.13 ± 0.02	NA	0.150 ± 0.001
5	2	11.28 ± 0.5	1.225 ± 0.005	4.138 ± 0.004	6.58 ± 0.01	0.36 ± 0.01	0.212 ± 0.001
100	2	12.31 ± 0.2	1.294 ± 0.004	4.214 ± 0.004	6.80 ± 0.01	0.22 ± 0.01	0.210 ± 0.001
250	2	12.97 ± 0.9	1.225 ± 0.003	4.680 ± 0.004	7.13 ± 0.02	0.17 ± 0.02	0.184 ± 0.001
500	2	14.17 ± 0.6	1.225 ± 0.003	4.762 ± 0.004	7.21 ± 0.02	0.18 ± 0.02	0.238 ± 0.001

Spherical polymersomes, when subjected to osmotic stress can undergo reduction in volume in two energetic pathways. Deflation can either proceed via prolates (elongated structures) or via oblates (disk shape). At low salt concentrations, where the impact of ion-membrane interactions can be negligible and the contribution from C_0 is negligible, the prolate pathway has a low energetic profile.[2, 31] The major driving force behind the shape transformation of the polymersome at low hypertonic conditions is the decrease in aqueous inner volume. In the suggested shape by Antonietti et al, once the volume -to- area reaches around 0.6 the spherical vesicles evolve to

represent elongated structures followed by formation of stomatocytes.[30] This pathway has been also suggested by Men et al. and Chakraboty et al. where the spherical polymersomes, first change to elongated forms followed by inward bending of the bilayer which eventually lead to non-spherical structures. [26, 33] The two ends of the stomatocytes could eventually fuse making nested vesicles. This could explain the co-existence of a larger number of elongated structures and few nested structures at 5 mM NaCl system. This data also agrees with literature where spherical polymersomes consist of PEG as the hydrophilic corona, undergo shape transformation to elongated structures when exposed to low NaCl concentrations.[31, 68] Table 02 reports an increment of PDMS shell thickness (δ_{PDMS}) with increasing salt concentration. This is due to the stretching of the membrane due to osmotic stress.[33] The formation of multi-vesicular structures at higher hypertonic stress levels can be explained as a combined effect of inner volume reduction and/or ion-membrane interactions. At high osmotic stress conditions, when the vesicles undergo further shrinkage membrane "budding" can occur to accommodate excess of surface membrane area of the inner membrane, creating multi-vesicular structures (Structure iv of Figure 9).[30, 69] Based from SAXS, it can be assumed that Na^+ and Cl^- ions interact with the PEG parts of the triblock copolymer since these blocks are exposed to the aqueous media. Binding of ions to the polymersome membrane can result in increased electrostatic repulsions increasing the inter-lamellar spacing (*d*) as reported in Table 02.

Therefore, we can assume that nested vesicles with small budding membrane within them, fuse together to form multi-vesicular structure when the salt concentration is further increased. As far as we know reports on formation of multi-vesicular structures at high salt

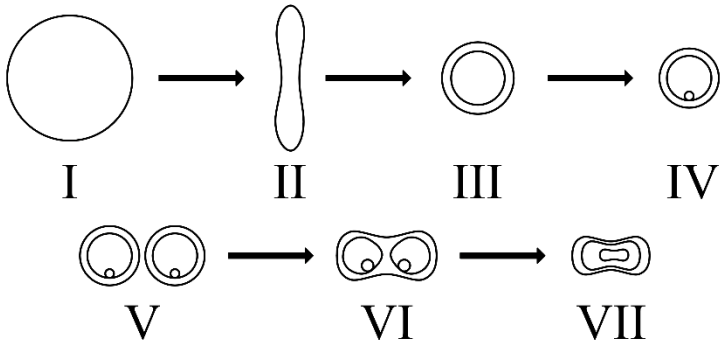

concentrations are scare. Therefore, more theoretical work is needed for more advanced explanation. In figure 8 we propose a tentative pathway for multi-vesicular structure formation. In the following we will discuss more in details.

Figure 8. Suggested vesicle shape transformation and vesicle fusion pathway for polymersomes with increasing NaCl concentration.

Effect of Cl^- Anion

An explanation based on chaotropic and kosmotropic ions frequently used in protein purification can be suggested to explain the fused and multi-vesicular vesicle structures. Chaotropic ions (weakly hydrated ions) destroy the relatively ordered structure of water molecules of the protein hydrate shell by interacting favorably with the protein surface.[70] This will denature the protein. Kosmotropic (strongly hydrated ions) ions have a strong interaction with water hence will move water surrounding the protein molecules to the bulk solution. This will disrupt the hydration barrier between proteins (hence dehydrate the protein surface) causing aggregation.[70, 71] Chloride anions known as a borderline kosmotropic/chaotropic agent and in the case of the polymersomes discussed here acted mainly as a kosmotropic anion.[72] Men and coworkers have suggested that there can be three types of interactions between monoanions and PEG polymer.[26] Based on that it can be assumed water molecules bound to Cl^- anion can form hydrogen bonds with the oxygen atom of polyethylene glycol units. (Figure 9 a). Charge distributions of common homopolymers with electron withdrawing heteroatoms like poly(propylene oxide) (PPO), poly(vinyl methyl ether) (PVME), and poly(N -isopropyl acrylamide) (PNIPAM) have been calculated based on density functional theory. The results showed that, heteroatoms (N or O) had a negative charge and the CH_n groups next to the heteroatoms showed a slightly positive charge.[73] We can assume that the same charge distribution exists in PEG and Cl^- anion can interact with the some slightly positively charged CH_2 units of the PEG via anion-dipole interactions (Figure 9 b). This may result in small anion-bound-regions and non-anion-bound-regions within the polymer chains. Non anion bound regions aggregate together and anion bound regions can stabilize the formed structure.[73, 74] The third type of interaction is where Cl^- ion can show a kosmotropic behavior and dehydrate the hydrophobic polymer backbone (Figure 9 c). This could provide individual polymer chains

bundling force to aggregate.[26] Considering the above three interacting pathways of Cl^- with PEG end blocks second and third types of interaction have more pronounced effect to facilitate membrane fusion by associating PEG polymer chains from different vesicle coronas in high NaCl concentrations.

Effect of Na^+ Cations

It has been proposed that strongly hydrated A-region of cations[75] can interact with the oxide groups of poly(ethylene oxide) of polymersome shell in the same manner as they would interact with NH_3 or any other basic molecule.[76]. This concept is based on the observation that enthalpies and entropies of dilution of PEG solutions with Na^+, Li^+ and Ca^{2+} ions are relatively less negative.[77] There is sufficient charge on oxide groups which causes PEG to be strongly hydrated and interact with cations.[78] The interactions between Na^+ and the oxide groups are strong enough so that the cations will bind directly the polymer [27, 76] (Figure). This would lead to formation of a pseudo-polyelectrolyte with non-ionic PEG. This pseudo-polyelectrolyte formation would make the polymer chains more mobile since now they have more favorable interactions with the solvent.[78, 79]

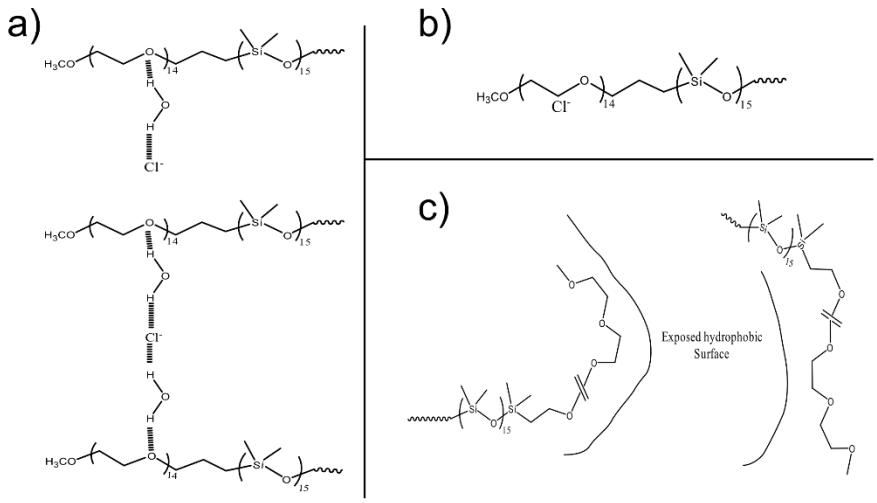

Figure 10. Possible interactions between PEG blocks and Cl^- anions in aqueous media (a) water molecules bound to Cl^- anions can form hydrogen bonds with oxygen atoms. (b) Cl^- anion can bind directly to the PEG and this will lead to ion accumulation at the polymer/water interface. (c) anions can interfere with the hydrophobic hydration of the polymer by increasing the surface tension of the cavity from the hydrophobic segment..[26]

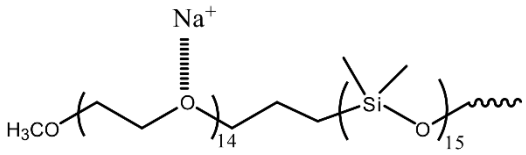

Figure 10. Possible interactions between PEG blocks and Na^+ cations in aqueous media: Na^+ can directly interact with the oxygen atom. [26]

CONCLUSION

In this work we have presented the synthesis of PEG – PDMS – PEG triblock copolymer which self-assemble into spherical polymersomes. These polymersomes can undergo rapid shrinkage upon addition of NaCl leading to multi-vesicular structures. We have used small angle neutron and

X-ray scattering to structural features of the polymersomes at nanoscopic length scale. We conclude that the shape and structural changes observed in the polymersomes are a combined result of osmotic pressure change and ion-membrane interactions. We have discussed in detail the possible interactions of Na^+ and Cl^- ions with the PEG parts of the triblock copolymer. Such polymersomes can offer excellent candidates for drug delivery mechanism where we can fine tune the formation of different layers by controlling osmotic change and fusion mechanism. The potential to manipulate the formation of different layers in polymersomes will allow us to store multiple drugs on separate layers which can help us to control the dose and rate of delivery over time.

AUTHOR INFORMATION

Corresponding Authors

*E-mail: g.sudipta26@gmail.com

*E-mail: gjschneider@lsu.edu

ORCID

Sudipta Gupta: 0000-0001-6642-3776

Gerald J. Schneider: 0000-0002-5577-9328

Rasangi M. Perera: 0000-0002-1394-4006

Notes

The authors declare no competing financial interest.

ACKNOWLEDGEMENT

The neutron scattering work is supported by the U.S. Department of Energy (DOE) under EPSCoR Grant No. DE-SC0012432 with additional support from the Louisiana Board of Regents. Access

to the neutron spin echo spectrometer and small-angle scattering instruments was provided by the Center for High Resolution Neutron Scattering, a partnership between the National Institute of Standards and Technology and the National Science Foundation under Agreement No. DMR-1508249. Use of the Stanford Synchrotron Radiation Lightsource, SLAC National Accelerator laboratory, is supported by the U.S. Department of Energy, Office of Science, Office of Basic Energy Sciences under Contract No. DE-AC0276SF00515. The SSRL Structural Molecular Biology Program is supported by the DOE Office of Biological and Environmental Research, and by the National Institute of General Medical Sciences (P30GM133894). The Pilatus detector at beamline 4-2 at SSRL was funded under National Institute of Health Grant S10OD021512. The contents of this publication are solely the responsibility of the authors and do not necessarily represent the official views of NIGMS or NIH. The polymer synthesis and characterization of this research was conducted at the Center for Nanophase Materials Sciences, which is a DOE Office of Science User Facility. We would like to thank Rafael Cueto (LSU) for his support in DLS experiments, Jibao He (Tulane University) for his support in Cryo-TEM, Jeff Krzywon at beamline NG7 at NIST for his support in SANS measurements and Thomas Weiss at Beamline 4-2 of the Stanford Synchrotron Radiation Lab (SSRL) for his support in SAXS measurements.

DISCLAIMER

Certain trade names and company products are identified in order to specify adequately the experimental procedure. In no case does such identification imply recommendation or endorsement by the National Institute of Standards and Technology, nor does it imply that the products are necessarily the best for the purpose. This paper was prepared as an account of work sponsored by an agency of the United States Government. Neither the United States Government nor any agency thereof, nor any of their employees, makes any warranty, express or implied, or assumes any legal liability or responsibility for the accuracy, completeness, or usefulness of any information, apparatus, product, or process disclosed, or represents that its use would not infringe privately owned rights. Reference herein to any specific commercial product, process, or service by trade name, trademark, manufacturer, or otherwise does not necessarily constitute or imply its endorsement, recommendation, or favoring by the United States Government or any agency thereof. The views and opinions of authors expressed herein do not necessarily state or reflect those of the United States Government or any agency thereof.

REFERENCES

1. Liu, F.; Kozlovskaya, V.; Medipelli, S.; Xue, B.; Ahmad, F.; Saeed, M.; Cropek, D.; Kharlampieva, E., Temperature-Sensitive Polymersomes for Controlled Delivery of Anticancer Drugs. *Chemistry of Materials* **2015,** *27* (23), 7945-7956.
2. Seifert, U.; Berndl, K.; Lipowsky, R., Shape transformations of vesicles: Phase diagram for spontaneous-curvature and bilayer-coupling models. *Physical Review A* **1991,** *44* (2), 1182-1202.
3. , P.; Driamov, S.; Ziegler, J.; Ben-Haim, N.; Marsch, S.; Meier, W.; Hunziker, P., Toward Intelligent Nanosize Bioreactors: A pH-Switchable, Channel-Equipped, Functional Polymer Nanocontainer. *Nano Letters* **2006,** *6* (10), 2349-2353 Broz.
4. Choi, H.-J.; Montemagno, C. D., Artificial Organelle: ATP Synthesis from Cellular Mimetic Polymersomes. *Nano Letters* **2005,** *5* (12), 2538-2542.
5. Tangorra, R. R.; Operamolla, A.; Milano, F.; Omar, O. H.; Henrard, J.; Comparelli, R.; Italiano, F.; Agostiano, A.; De Leo, V.; Marotta, R.; Falqui, A.; Farinola, G. M.; Trotta, M., Assembly of a photosynthetic reaction center with ABA tri-block polymersomes: highlights on protein localization. *Photochemical & Photobiological Sciences* **2015,** *14* (10), 1844-1852.
6. Ahmed, F.; Photos, P. J.; Discher, D. E., Polymersomes as viral capsid mimics. 2006; Vol. 67, pp 4-14.
7. Levine, D. H.; Ghoroghchian, P. P.; Freudenberg, J.; Zhang, G.; Therien, M. J.; Greene, M. I.; Hammer, D. A.; Murali, R., Polymersomes: A new multi-functional tool for cancer diagnosis and therapy. *Methods* **2008,** *46* (1), 25-32.
8. De Oliveira, H.; Thevenot, J.; Lecommandoux, S., Smart polymersomes for therapy and diagnosis: fast progress toward multifunctional biomimetic nanomedicines. *WIREs Nanomedicine and Nanobiotechnology* **2012,** *4* (5), 525-546.
9. Discher, B. M.; Won, Y.-Y.; Ege, D. S.; Lee, J. C.-M.; Bates, F. S.; Discher, D. E.; Hammer, D. A., Polymersomes: Tough Vesicles Made from Diblock Copolymers. *Science* **1999,** *284* (5417), 1143-1146.
10. Leong, J.; Teo, J. Y.; Aakalu, V. K.; Yang, Y. Y.; Kong, H., Engineering Polymersomes for Diagnostics and Therapy. *Adv Healthc Mater* **2018,** *7* (8), e1701276.
11. Xu, F.; Li, X.; Huang, X.; Pan, J.; Wang, Y.; Zhou, S., Development of a pH-responsive polymersome inducing endoplasmic reticulum stress and autophagy blockade. *Science Advances* **2020,** *6* (31), eabb8725.
12. Kozlovskaya, V.; Liu, F.; Yang, Y.; Ingle, K.; Qian, S.; Halade, G. V.; Urban, V. S.; Kharlampieva, E., Temperature-Responsive Polymersomes of Poly(3-methyl-N-vinylcaprolactam)-block-poly(N-vinylpyrrolidone) To Decrease Doxorubicin-Induced Cardiotoxicity. *Biomacromolecules* **2019,** *20* (10), 3989-4000.
13. Champion, J. A.; Katare, Y. K.; Mitragotri, S., Particle shape: a new design parameter for micro- and nanoscale drug delivery carriers. *J Control Release* **2007,** *121* (1-2), 3-9.
14. Chauhan, V. P.; Popovic, Z.; Chen, O.; Cui, J.; Fukumura, D.; Bawendi, M. G.; Jain, R. K., Fluorescent nanorods and nanospheres for real-time in vivo probing of nanoparticle shape-dependent tumor penetration. *Angew Chem Int Ed Engl* **2011,** *50* (48), 11417-20.
15. Decuzzi, P.; Pasqualini, R.; Arap, W.; Ferrari, M., Intravascular delivery of particulate systems: does geometry really matter? *Pharm Res* **2009,** *26* (1), 235-43.
16. Sharma, G.; Valenta, D. T.; Altman, Y.; Harvey, S.; Xie, H.; Mitragotri, S.; Smith, J. W., Polymer particle shape independently influences binding and internalization by macrophages. *J Control Release* **2010,** *147* (3), 408-12.
17. Kawaguchi, H.; Koiwai, N.; Ohtsuka, Y.; Miyamoto, M.; Sasakawa, S., Phagocytosis of latex particles by leucocytes. I. Dependence of phagocytosis on the size and surface potential of particles. *Biomaterials* **1986,** *7* (1), 61-66.
18. Tabata, Y.; Ikada, Y., Effect of the size and surface charge of polymer microspheres on their phagocytosis by macrophage. *Biomaterials* **1988,** *9* (4), 356-362.
19. Hsieh, D. S. T.; Rhine, W. D.; Langer, R., Zero-Order Controlled-Release Polymer Matrices for Micro- and Macromolecules. *Journal of Pharmaceutical Sciences* **1983,** *72* (1), 17-22.
20. Champion, J. A.; Mitragotri, S., Role of target geometry in phagocytosis. *Proceedings of the National Academy of Sciences of the United States of America* **2006,** *103* (13), 4930-4934.
21. Moghimi, S. M.; Hunter, A. C.; Murray, J. C., Long-circulating and target-specific nanoparticles: Theory to practice. 2001; Vol. 53, pp 283-318.

22. Rikken, R. S.; Engelkamp, H.; Nolte, R. J.; Maan, J. C.; van Hest, J. C.; Wilson, D. A.; Christianen, P. C., Shaping polymersomes into predictable morphologies via out-of-equilibrium self-assembly. *Nat Commun* **2016,** *7*, 12606.
23. Rikken, R. S.; Kerkenaar, H. H.; Nolte, R. J.; Maan, J. C.; van Hest, J. C.; Christianen, P. C.; Wilson, D. A., Probing morphological changes in polymersomes with magnetic birefringence. *Chem Commun (Camb)* **2014,** *50* (40), 5394-6.
24. van Oers, M. C. M.; Rutjes, F. P. J. T.; van Hest, J. C. M., Tubular Polymersomes: A Cross-Linker-Induced Shape Transformation. *Journal of the American Chemical Society* **2013,** *135* (44), 16308-16311.
25. Yildirim, T.; Traeger, A.; Sungur, P.; Hoeppener, S.; Kellner, C.; Yildirim, I.; Pretzel, D.; Schubert, S.; Schubert, U. S., Polymersomes with Endosomal pH-Induced Vesicle-to-Micelle Morphology Transition and a Potential Application for Controlled Doxorubicin Delivery. *Biomacromolecules* **2017,** *18* (10), 3280-3290.
26. Men, Y.; Li, W.; Lebleu, C.; Sun, J.; Wilson, D. A., Tailoring Polymersome Shape Using the Hofmeister Effect. *Biomacromolecules* **2020,** *21* (1), 89-94.
27. Men, Y.; Li, W.; Janssen, G. J.; Rikken, R. S. M.; Wilson, D. A., Stomatocyte in Stomatocyte: A New Shape of Polymersome Induced via Chemical-Addition Methodology. *Nano Lett* **2018,** *18* (3), 2081-2085.
28. Wong, C. K.; Stenzel, M. H.; Thordarson, P., Non-spherical polymersomes: formation and characterization. *Chem Soc Rev* **2019,** *48* (15), 4019-4035.
29. Mui, B. L.; Döbereiner, H. G.; Madden, T. D.; Cullis, P. R., Influence of transbilayer area asymmetry on the morphology of large unilamellar vesicles. *Biophysical Journal* **1995,** *69* (3), 930-941.
30. Antonietti, M.; Förster, S., Vesicles and Liposomes: A Self-Assembly Principle Beyond Lipids. *Advanced Materials* **2003,** *15* (16), 1323-1333.
31. Abdelmohsen, L. K.; Williams, D. S.; Pille, J.; Ozel, S. G.; Rikken, R. S.; Wilson, D. A.; van Hest, J. C., Formation of Well-Defined, Functional Nanotubes via Osmotically Induced Shape Transformation of Biodegradable Polymersomes. *J Am Chem Soc* **2016,** *138* (30), 9353-6.
32. Rikken, R. S. M.; Engelkamp, H.; Nolte, R. J. M.; Maan, J. C.; van Hest, J. C. M.; Wilson, D. A.; Christianen, P. C. M., Shaping polymersomes into predictable morphologies via out-of-equilibrium self-assembly. *Nature Communications* **2016,** *7* (8), 12606.
33. Chakraborty, K.; Shinoda, W.; Loverde, S. M., Molecular simulation of the shape deformation of a polymersome. *Soft Matter* **2020,** *16* (13), 3234-3244.
34. Paxton, W., Control of mechanically activated polymersome fusion: Factors affecting fusion. *Journal of Polymer Science Part B: Polymer Physics* **2014,** *53* (4).
35. Ionescu, M.; Winton, B.; Wexler, D.; Siegele, R.; Deslantes, A.; Stelcer, E.; Atanacio, A.; Cohen, D. D., Enhanced biocompatibility of PDMS (polydimethylsiloxane) polymer films by ion irradiation. *Nuclear Instruments and Methods in Physics Research Section B: Beam Interactions with Materials and Atoms* **2012,** *273*, 161-163.
36. Badi, N., Non-linear PEG-based thermoresponsive polymer systems. *Progress in Polymer Science* **2017,** *66*, 54-79.
37. De Mel, J. U.; Gupta, S.; Perera, R. M.; Ngo, L.; Zolnierczuk, P.; Bleuel, M.; Pingali, S. V.; Schneider, G. J., Influence of External NaCl Salt on Membrane Rigidity of Neutral DOPC Vesicles. *Langmuir* **2020,** *36* (32), 9356-9367.
38. Gupta, S.; Camargo, M.; Stellbrink, J.; Allgaier, J.; Radulescu, A.; Lindner, P.; Zaccarelli, E.; Likos, C. N.; Richter, D., Dynamic phase diagram of soft nanocolloids. *Nanoscale* **2015,** *7* (33), 13924-34.
39. Gupta, S.; De Mel, J. U.; Perera, R. M.; Zolnierczuk, P.; Bleuel, M.; Faraone, A.; Schneider, G. J., Dynamics of Phospholipid Membranes beyond Thermal Undulations. *J Phys Chem Lett* **2018,** *9*, 2956-2960.
40. Sternhagen, G. L.; Gupta, S.; Zhang, Y.; John, V.; Schneider, G. J.; Zhang, D., Solution Self-Assemblies of Sequence-Defined Ionic Peptoid Block Copolymers. *Journal of American Chemical Society* **2018,** *140* (11), 4100-4109.
41. De Mel, J. U.; Gupta, S.; Willner, L.; Allgaier, J.; Stingaciu, L. R.; Bleuel, M.; Schneider, G. J., Manipulating Phospholipid Vesicles at the Nanoscale: A Transformation from Unilamellar to Multilamellar by an n-Alkyl-poly(ethylene oxide). *Langmuir* **2021,** *37* (7), 2362-2375.
42. Nallet, F.; Laversanne, R.; Roux, D., Modelling X-ray or Neutron Scattering Spectra of Lyotropic Lamellar Phases: Interplay Between Form and Structure Factors. *Journal de Physique II* **1993,** *3*, 16.
43. Berghausen, J.; Zipfel, J.; Lindner, P.; Richtering, W., Influence of Water-Soluble Polymers on the Shear-Induced Structure Formation in Lyotropic Lamellar Phases. *The Journal of Physical Chemistry B* **2001,** *105* (45), 11081-11088.

44. Glinka, C. J.; Barker, J. G.; Hammouda, B.; Krueger, S.; Moyer, J. J.; Orts, W. J., The 30 m Small-Angle Neutron Scattering Instruments at the National Institute of Standards and Technology. *Journal of Applied Crystallography* **1998,** *31* (3), 430-445.
45. Choi, S. M.; Barker, J. G.; Glinka, C. J.; Cheng, Y. T.; Gammel, P. L., Focusing cold neutrons with multiple biconcave lenses for small-angle neutron scattering. *Journal of Applied Crystallography* **2000,** *33* (3), 793-796.
46. Kline, S. R., Reduction and analysis of SANS and USANS data using IGOR Pro. *Journal of Applied Crystallography* **2006,** *39* (6), 895-900.
47. Glatter, O.; Kratky, O., *Small angle x-ray scattering*. Academic Press Inc. Ltd. : London, 1982.
48. P. Lindner; Th. Zemb, *Neutron, X-rays and Light: Scattering Methods Applied to Soft Condensed Matter*. 1st ed.; Elsevier Science: Amsterdam, 2002.
49. Orthaber, D.; Bergmann, A.; Glatter, O., SAXS experiments on absolute scale with Kratky systems using water as a secondary standard. *Journal of Applied Crystallography* **2000,** *33* (2), 218-225.
50. Pencer, J.; White, G. F.; Hallett, F. R., Osmotically Induced Shape Changes of Large Unilamellar Vesicles Measured by Dynamic Light Scattering. *Biophysical Journal* **2001,** *81* (5), 2716-2728.
51. Boroske, E.; Elwenspoek, M.; Helfrich, W., Osmotic shrinkage of giant egg-lecithin vesicles. *Biophysical Journal* **1981,** *34* (1), 95-109.
52. Chang, H.-Y.; Lin, Y.-L.; Sheng, Y.-J.; Tsao, H.-K., Structural Characteristics and Fusion Pathways of Onion-Like Multilayered Polymersome Formed by Amphiphilic Comb-Like Graft Copolymers. *Macromolecules* **2013,** *46* (14), 5644-5656.
53. Luo, J.; Liu, T.; Qian, K.; Wei, B.; Hu, Y.; Gao, M.; Sun, X.; Lin, Z.; Chen, J.; Bera, M. K.; Chen, Y.; Zhang, R.; Mao, J.; Wesdemiotis, C.; Tsige, M.; Cheng, S. Z. D.; Liu, T., Continuous Curvature Change into Controllable and Responsive Onion-like Vesicles by Rigid Sphere-Rod Amphiphiles. *ACS Nano* **2020,** *14* (2), 1811-1822.
54. Gerstl, C.; Brodeck, M.; Schneider, G. J.; Su, Y.; Allgaier, J.; Arbe, A.; Colmenero, J.; Richter, D., Short and Intermediate Range Order in Poly(alkylene oxide)s. A Neutron Diffraction and Molecular Dynamics Simulation Study. *Macromolecules* **2012,** *45* (17), 7293-7303.
55. Yamada, L. N.; Seto, H.; Takeda, T.; Nagao, M.; Kawabata, Y.; Inoue, K., SAXS, SANS and NSE Studies on "Unbound State" in DPPC/Water/CaCl2System. *Journal of the Physical Society of Japan* **2005,** *74* (10), 2853-2859.
56. De Mel, J. U.; Gupta, S.; Perera, R. M.; Ngo, L. T.; Zolnierczuk, P.; Bleuel, M.; Pingali, S. V.; Schneider, G. J., Influence of external NaCl salt on membrane rigidity of neutral DOPC vesicles. *Langmuir* **2020,** *36*, 9356−9367.
57. Leneveu, D. M.; Rand, R. P.; Parsegian, V. A., Measurement of forces between lecithin bilayers. *Nature* **1976,** *259*, 601– 603.
58. Salva, R.; Le Meins, J. F.; Sandre, O.; Brulet, A.; Schmutz, M.; Guenoun, P.; Lecommandoux, S., Polymersome shape transformation at the nanoscale. *ACS Nano* **2013,** *7* (10), 9298-311.
59. Frédéric, C.; Annie, B.; Julian, O.; Yves, G.; Olivier, M.-M.; Lecommandoux, S., Structure of Polypeptide Based Diblock Copolymers in Solution: Stimuli-responsive Vesicles and Micelles. *Langmuir* **2005,** *21* (10), 4308–4315.
60. Yang, Y.; Alford, A.; Kozlovskaya, V.; Zhao, S.; Joshi, H.; Kim, E.; Qian, S.; Urban, V.; Cropek, D.; Aksimentiev, A.; Kharlampieva, E., Effect of temperature and hydrophilic ratio on the structure of poly(N-vinylcaprolactam)-block-poly(dimethylsiloxane)-block-poly(N-vinylcaprolact am) polymersomes. *ACS Appl Polym Mater* **2019,** *1* (4), 722-736.
61. Devanand, K.; Selser, J. C., Asymptotic behavior and long-range interactions in aqueous solutions of poly(ethylene oxide). *Macromolecules* **1991,** *24* (22), 5943-5947.
62. M. Rubinstein; Ralph H. Colby, *Polymer Physics*. Oxford University Press: New York, 2003.
63. Fauquignon, M.; Ibarboure, E.; Carlotti, S.; Brulet, A.; Schmutz, M.; Le Meins, J. F., Large and Giant Unilamellar Vesicle(s) Obtained by Self-Assembly of Poly(dimethylsiloxane)-b-poly(ethylene oxide) Diblock Copolymers, Membrane Properties and Preliminary Investigation of their Ability to Form Hybrid Polymer/Lipid Vesicles. *Polymers (Basel)* **2019,** *11* (12).
64. Itel, F.; Chami, M.; Najer, A.; Lörcher, S.; Wu, D.; Dinu, I. A.; Meier, W., Molecular Organization and Dynamics in Polymersome Membranes: A Lateral Diffusion Study. *Macromolecules* **2014,** *47* (21), 7588-7596.
65. Rideau, E.; Dimova, R.; Schwille, P.; Wurm, F. R.; Landfester, K., Liposomes and polymersomes: a comparative review towards cell mimicking. *Chemical Society Reviews* **2018,** *47* (23), 8572-8610.
66. Chabanon, M.; Ho, J. C. S.; Liedberg, B.; Parikh, A. N.; Rangamani, P., Pulsatile Lipid Vesicles under Osmotic Stress. *Biophys J* **2017,** *112* (8), 1682-1691.

67. Petrache, H. I.; Tristram-Nagle, S.; Harries, D.; Kucerka, N.; Nagle, J. F.; Parsegian, V. A., Swelling of phospholipids by monovalent salt. *J Lipid Res* **2006,** *47* (2), 302-309.
68. Ridolfo, R.; Williams, D. S.; van Hest, J. C. M., Influence of surface charge on the formulation of elongated PEG-b-PDLLA nanoparticles. *Polymer Chemistry* **2020,** *11* (16), 2775-2780.
69. Salva, R.; Le Meins, J.-F.; Sandre, O.; Brûlet, A.; Schmutz, M.; Guenoun, P.; Lecommandoux, S., Polymersome Shape Transformation at the Nanoscale. *ACS Nano* **2013,** *7* (10), 9298-9311.
70. Bogar, F.; Bartha, F.; Nasztor, Z.; Fabian, L.; Leitgeb, B.; Der, A., On the Hofmeister effect: fluctuations at the protein-water interface and the surface tension. *J Phys Chem B* **2014,** *118* (29), 8496-504.
71. Pegram, L. M.; Record, M. T., Partitioning of atmospherically relevant ions between bulk water and the water/vapor interface. *Proceedings of the National Academy of Sciences* **2006,** *103* (39), 14278-14281.
72. Zongo, L.; Lange, H.; Crestini, C., A Study of the Effect of Kosmotropic and Chaotropic Ions on the Release Characteristics of Lignin Microcapsules under Stimuli-Responsive Conditions. *ACS Omega* **2019,** *4* (4), 6979-6993.
73. Li, J.; Wang, X.; Zhang, T.; Wang, C.; Huang, Z.; Luo, X.; Deng, Y., A review on phospholipids and their main applications in drug delivery systems. *Asian Journal of Pharmaceutical Sciences* **2015,** *10* (2), 81-98.
74. Collins, K. D., The behavior of ions in water is controlled by their water affinity. *Quarterly Reviews of Biophysics* **2019,** *52*, e11.
75. Frank, H. S.; Wen, W.-Y., Ion-solvent interaction. Structural aspects of ion-solvent interaction in aqueous solutions: a suggested picture of water structure. *Discussions of the Faraday Society* **1957,** *24* (0), 133-140.
76. Erlander, S. R., The production of pseudo-polyelectrolytes in aqueous salt solutions of nonionic polymers. *Journal of Colloid and Interface Science* **1970,** *34* (1), 53-64.
77. Dobbie, J. W.; Evans, R.; Gibson, D. V.; Smitham, J. B.; Napper, D. H., Enhanced steric stabilization. *Journal of Colloid and Interface Science* **1973,** *45* (3), 557-565.
78. Liu, K.-J.; Parsons, J. L., Solvent Effects on the Preferred Conformation of Poly (ethylene glycols). *Macromolecules* **1969,** *2* (5), 529-533.
79. Liu, K.-J.; Anderson, J. E., Nuclear Magnetic Relaxation in Poly(ethylene oxide)-Salt Solutions. *Macromolecules* **1969,** *2*, 235.